Monthly Notices
of the
ROYAL ASTRONOMICAL SOCIETY
MNRAS **490,** 3440–3447 (2019) doi:10.1093/mnras/stz2806

Concurrent effect of Alfvén waves and planar magnetic structure on geomagnetic storms

Zubair I. Shaikh [1★], Anil Raghav [2★], Geeta Vichare,[1★] Ankush Bhaskar,[3,4] Wageesh Mishra[5] and Komal Choraghe[2]

[1] *Indian Institute of Geomagnetism (IIG), New Panvel, Navi, Mumbai-410218, India*
[2] *University Department of Physics, University of Mumbai, Vidyanagari, Santacruz (E), Mumbai-400098, India*
[3] *Heliophysics Science Division, NASA/Goddard Space Flight Center, Greenbelt, MD, USA*
[4] *University Corporation for Atmospheric Research, Boulder, CO 80307-3000, USA*
[5] *Max Planck Institute for Solar System Research, Justus-von-Liebig-Weg 3, D-37077 Göttingen, Germany*

Accepted 2019 October 1. Received 2019 September 26; in original form 2019 August 28

ABSTRACT

Generally, interplanetary coronal mass ejection (ICME) triggers intense and strong geomagnetic storms. It has been established that the ICME sheath-moulded planar magnetic structure enhances the amplitude of the storms. Alfvén waves embedded in ICME magnetic clouds or high solar streams including corotating interacting regions (CIRs) in turn extend the recovery phase of the storm. Here, we investigate a geomagnetic storm with a very complex temporal profile with multiple decreasing and recovery phases. We examine the role of planar magnetic structure (PMS) and Alfvén waves in the various phases of the storm. We find that fast decrease and fast recovery phases are evident during transit of PMS regions, whereas a slight decrease or recovery is found during the transit of regions embedded with Alfvénic fluctuations.

Key words: magnetic reconnection – Sun: coronal mass ejections (CMEs) – Sun: magnetic fields – solar wind.

1 INTRODUCTION

The plasma emitted during solar transients has been responsible for the development of three major current systems in the magnetosphere/ionosphere of the Earth, namely, the Chapman–Ferraro current (Chapman & Ferraro 1931; Chapman 1933), the ring current (Axford & Hines 1961; Dungey 1961; Akasofu, Chapman & Venkatesan 1963), and the auroral electro-jet (Akasofu, Chapman & Meng 1965; Davis & Sugiura 1966). These currents have been observed in the form of geomagnetic disturbances on the Earth (Akasofu 1963; Kamide et al. 1998; Akasofu 2018). During geomagnetic disturbance, the horizontal component (H) of the Earth's magnetic field shows a decrease for a few hours followed by subsequent recovery; this is termed geomagnetic storm phenomena (Chapman & Bartels 1940; Gonzalez & Tsurutani 1987; Gosling et al. 1990; Gonzalez et al. 1994; Kamide et al. 1998).

In general, the temporal profile of geomagnetic storms is divided into different phases such as (1) sudden storm commencement (SSC) followed by the initial phase, (2) main phase, and (3) recovery phase (Kamide et al. 1998; Akasofu 2011, 2018). The intensification of the Chapman–Ferraro current (magnetopause current) on the boundary surface of the magnetosphere is the leading cause of SSC and the initial phase of the storm (Chapman & Ferraro 1931; Chapman 1933). It is suggested that the increased solar wind dynamic pressure drives the magnetopause inwards up to four Earth radii, which leads to strengthening of the magnetopause current and a sudden definite increase in the H component (Dessler, Francis & Parker 1960). During the main phase of the storm, charged particles from the near-Earth plasma sheet are energized and injected more deeply into the inner magnetosphere, producing the storm-time ring current (westward direction), and causing a depressed H component for a few hours (Frank 1967; Smith & Hoffman 1973; Williams 1983; Daglis et al. 1999; Kozyra & Liemohn 2003). This is measured at low-latitude stations with magnetometers as the disturbance storm-time index (D_{st}, 1 h temporal resolution) or by the symmetric ring-current intensity index (SYM-H, 1 min temporal resolution) (Gonzalez et al. 1994). The recovery phase of the storm occurs due to decay in the ring current either by charge exchange (Prölss 1973; Keika et al. 2006), Coulomb interaction or wave–particle interaction processes (Kozyra et al. 1997; Yermolaev et al. 2012). Akasofu et al. (1963) reported that the recovery phase of an intense storm has two different characteristics, (i) fast recovery at the beginning and (ii) slowing down later, and needs at least two exponential functions to explain this (Akasofu 2018).

Geomagnetic storms occur when the interplanetary magnetic field (IMF) turns southward and remains southward for an prolonged period of time. The south component of the IMF (B_z) controls the

★ E-mail: zubairshaikh584@gmail.com (ZIS); raghavanil1984@gmail.com (AR); vicharegeeta@gmail.com (GV)

© 2019 The Author(s)
Published by Oxford University Press on behalf of the Royal Astronomical Society

Downloaded from https://academic.oup.com/mnras/article/490/3/3440/5610655 by Inter-University Centre for Astronomy and Astrophysics user on 04 May 2023

reconnection rate between the magnetic field lines of interplanetary space and magnetosphere. Hence, it regulates the growth/decay of the storm (or ring current) (Dungey 1961; Fairfield & Cahill 1966; Kamide et al. 1998; Gonzalez et al. 1994; O'Brien & McPherron 2000; Milan, Gosling & Hubert 2012). The main identified solar wind conditions responsible for the aforementioned scenario are (1) interplanetary counterparts of coronal mass ejections (ICMEs) (Lindsay, Russell & Luhmann 1995; Kamide et al. 1998; Gonzalez, Tsurutani & De Gonzalez 1999; Kilpua, Koskinen & Pulkkinen 2017a), (2) corotating interaction regions (CIRs) (Tsurutani et al. 2006; Richardson 2018), (3) Alfvén-wave-embedded solar wind streams (Tsurutani & Gonzalez 1987; Tsurutani et al. 1988; Tsurutani & Gonzalez 1997; Zhang et al. 2014), (4) interplanetary small-scale magnetic flux ropes (Moldwin et al. 2000; Feng et al. 2008), and (5) high-speed streams (HSS) from coronal holes (Krieger, Timothy & Roelof 1973; Sheeley, Harvey & Feldman 1976; Hansen, Hansen & Sawyer 1976). Out of these, in general, ICMEs are responsible for strong/extreme geomagnetic storms with significantly enhanced ring currents and intense auroras (Gonzalez & Tsurutani 1987; Gonzalez et al. 1994; Lepping et al. 1997; Akasofu 2011; Raghav et al. 2018), whereas storms caused by CIRs are normally moderate/weaker with less intensive auroras (Tsurutani & Gonzalez 1997).

Here, it is essential to note that the ICMEs have two major subparts, namely shock–sheath and magnetic clouds (MC) (Burlaga et al. 1981; Burlaga, Lepping & Jones 1990; Zurbuchen & Richardson 2006; Siscoe & Odstrcil 2008; Webb & Howard 2012; Tsurutani et al. 2011; Kilpua et al. 2017a). The features of the storm observed during the transit of ICME substructure, i.e. shock–sheath and MC are different in many aspects. An MC-driven storm has (1) substantial ring-current enhancement, (2) a much slower increase in auroral activity, (3) a more symmetric ring current, and (4) less intense field stretching and convection, whereas storms driven by sheath regions have (1) stronger auroral activity, (2) stronger magneto-tail field stretching, (3) larger asymmetry in the inner magnetosphere field configuration, and (4) a larger asymmetric ring current (see e.g. Huttunen, Koskinen & Schwenn 2002; Huttunen & Koskinen 2004; Huttunen et al. 2006; Pulkkinen et al. 2007; Tsurutani et al. 2011 and references therein).

In addition to this, planar magnetic structures (PMSs), i.e. the ordering of the magnetic field vector into a fixed plane, are identified within the ICME shock–sheath region (Nakagawa, Nishida & Saito 1989; Nakagawa 1993; Hakamada 1998; Neugebauer, Clay & Gosling 1993; Jones, Balogh & Horbury 1999; Palmerio, Kilpua & Savani 2016; Shaikh et al. 2018). A recent statistical study suggests that PMSs are more likely to drive geomagnetic storms (Palmerio et al. 2016). High compression in PMS strengthens the IMF B_z in a southward/northward direction at the cost of ecliptic components (B_x, B_y) (McComas et al. 1988, 1989; Palmerio et al. 2016). Recently, Kataoka et al. (2015) proposed that a double compression mechanism induced by PMS caused the St Patrick's Day intense geomagnetic storm of 2015 March.

Besides this, the various studies in the literature suggest that Alfvénic fluctuations amplify the IMF B_z component of the solar wind, which leads to an increase in the day-side reconnection electric field during geomagnetic storms (see e.g. Gonzalez et al. 1999; Richardson et al. 2006 and reference therein). The Alfvén wave is the most stable incompressible magneto-hydrodynamic (MHD) wave, often found in the solar wind and identified in ICME magnetic clouds (Belcher & Davis 1971; Eastwood et al. 2005; Marsch 2006; Cramer 2011; Bruno & Carbone 2013; Yang & Chao 2013; Raghav & Shaikh 2018; Raghav et al. 2018). Alfvén waves are suggested to be responsible for the long recovery phase of CIR-induced (Tsurutani & Gonzalez 1987; Tsurutani et al. 2006; Kasahara et al. 2009; Zhang et al. 2014) and ICME-induced (Raghav et al. 2018; Raghav, Choraghe & Shaikh 2019) geomagnetic storms. High-speed streams filled with Alfvénic fluctuations cause high-intensity long-duration continuous auroral electro-jet activity (HILDCAA), possibly due to the southward component of the Alfvén wave (Tsurutani & Gonzalez 1987; Tsurutani et al. 2006; Guarnieri 2006).

In summary, we note that the role of ICME (shock–sheath and MC) in geomagnetic storms has been intensively studied (Tsurutani et al. 1988; Kamide et al. 1998; Huttunen & Koskinen 2004; Oliveira & Raeder 2014; Lugaz et al. 2016; Kilpua et al. 2017a,b). Recently, the embedded fine structures within the shock–sheath or MC, i.e. the existence of PMS or Alfvén waves, has been investigated in detail. These fine structures are very important to understand the ICME's morphology (Jones et al. 2002), propagation and acceleration of energetic particles (Reames 1999; Sanderson et al. 2000; Manchester et al. 2005), and cosmic ray modulation, i.e. Forbush decrease (Raghav et al. 2014; Bhaskar, Subramanian & Vichare 2016b; Bhaskar et al. 2016a; Raghav et al. 2017; Shaikh, Raghav & Bhaskar 2017; Shaikh et al. 2018). In fact, the role of these fine structures during geomagnetic storms has also been studied independently (Kataoka et al. 2015; Palmerio et al. 2016; Raghav et al. 2018). Recently, we have reported a unique feature of the ICME sheath, i.e. the coexistence of PMS and Alfvénic fluctuations. Here, we study their influence on the topology of a geomagnetic storm profile in detail.

2 OBSERVATION

The studied ICME crossed the *Wind* spacecraft on 2000 October 12. The temporal variation of *in situ* plasma parameters during the ICME transit is shown in Fig. 1. We have used 1 min resolution *in situ* interplanetary data from the OMNI database available at https://cdaweb.sci.gsfc.nasa.gov/index.html/. The ICME substructures, i.e. shock–sheath and MC, are shown in different colour bands (see Fig. 1). The onset of the shock front is identified as sudden sharp enhancement in IMF $B_{\rm mag}$, solar wind speed (V_p), proton temperature (T) and proton density (N_p) (see the first vertical black dashed line). The shock front is followed by high N_p, T, V_p, and plasma beta (β) and large fluctuations in the IMF vector (i.e. $B_{x,\,y,\,z}$) region, which corresponds to the ICME shock–sheath (Shaikh et al. 2017; Kilpua et al. 2017a). The estimated thickness of the ICME shock–sheath is about 0.21 au, which is calculated by multiplying the average solar wind velocity ($\sim$450 km s^{-1}) by total time duration ($\sim$19.5 h). Information about the shock at 1 au observed by the *Wind* spacecraft is available at https://www.cfa.harvard.edu/shocks/wi_data/00179/wi_00179.html. Their analysis suggests that it is a fast forward (FF) shock with the following average properties: the shock normal $\hat{n} = (-0.968, -0.098, 0.170)$, and the angle between the shock normal and the magnetic field $\theta_{Bn} = 71.5^{\circ}$. This implies that the shock is a quasi-perpendicular shock. After the passage of the sheath, we observe a decrease in fluctuations in $B_{\rm mag}$ and $B_{\rm comp}$, a slow variation in θ and ϕ, and a slow steady trend in V_p and low β, indicating the transit of MC (Zurbuchen & Richardson 2006). The catalogue available at http://space.ustc.edu.cn/dreams/wind_icmes/ corroborates the identified boundary of MC.

In the present paper, we study an ICME-induced moderate geomagnetic storm with SYM-H $= -101$ nT that occurred on 2000 October 12. The ICME (shock–sheath + MC) transit time is $\sim$1.81 d and that of the geomagnetic storm is $\sim$3.08 d. The observed storm

Downloaded from https://academic.oup.com/mnras/article/490/3/3440/5610655 by Inter-University Centre for Astronomy and Astrophysics user on 04 May 2023

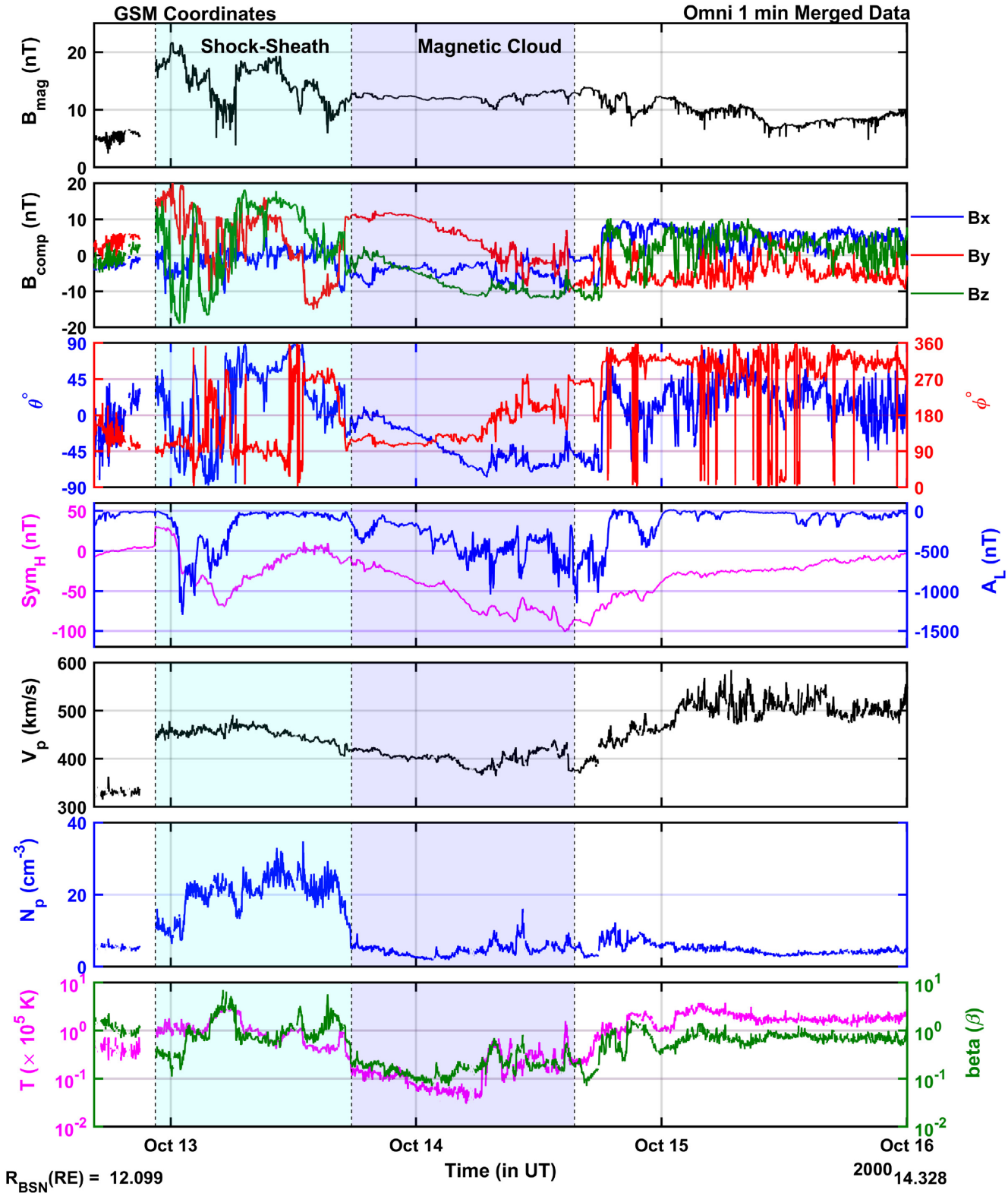

Figure 1. ICME crossed the Earth during 2000 October 12–14. The figure has seven sub-panels. The first and second panels show the temporal variation of IMF $B_{\rm mag}$ and $B_{\rm vec}$ (i.e. B_x, B_y and B_z). The third panel represents the azimuth (ϕ) and elevation (θ) angles of the IMF vector. The fourth panel expresses the temporal variation of the geomagnetic index, i.e. SYM-H and the A_L index. The fifth and sixth panels show solar wind speed (V_p) and plasma density (N_p). The seventh panel gives the temporal evolution of temperature (T_p) and plasma beta (β) respectively. Sudden storm commencement is shown by the first vertical black dashed line. The shock–sheath and MC regions are separated by different colour bands.

Downloaded from https://academic.oup.com/mnras/article/490/3/3440/5610655 by Inter-University Centre for Astronomy and Astrophysics user on 04 May 2023

profile is complex (not similar to the standard profile, as discussed in the introduction). Therefore, we divided the geomagnetic storm into five different regions (as shown in the bottom panel of Fig. 3) depending upon the decreasing and recovering phase of the SYM-H profile.

2.1 PMS analysis

PMS identification analysis was performed for each aforementioned region of the storm independently. We have utilized the following criteria/method as discussed in the literature for the PMS identification: (1) a wide distribution of the azimuth angle (i.e. $0^\circ < \phi < 360^\circ$), (2) good planarity, i.e. $\frac{|B_n|}{B} \leq 0.2$ (B is the magnitude of the IMF and B_n is the component of the magnetic field normal to the PMS plane, i.e. $B_n = \vec{B} \cdot \vec{n}$); this confirms the two-dimensionality, and (3) good efficiency $R = \frac{\lambda_2}{\lambda_3} \geq 3$ respectively (Nakagawa et al. 1989; Nakagawa 1993; Neugebauer et al. 1993; Jones et al. 1999; Jones & Balogh 2001; Palmerio et al. 2016; Shaikh et al. 2018). Here, λ_1, λ_2, and λ_3 are eigenvalues and $\hat{n}$ is the PMS normal direction calculated after minimum and maximum variance analysis (MVA) (Lepping & Behannon 1980; Sonnerup & Scheible 1998). A region issaid to be perfect plane when $B_n = 0$; therefore a low value of $\frac{|B_n|}{B}$ is a good indicator that the vectors are almost parallel to a plane (Neugebauer et al. 1993; Palmerio et al. 2016).

Each sub-figure of Fig. 2 depicts a wide wave-like distribution (i.e. azimuth angle spread over $0^\circ < \phi < 360^\circ$) of θ and ϕ. However, it is noted that only the sub-figures (a), (b) and (d) satisfy all of the criteria discussed above, while the other sub-plots, i.e. (c) and (e), do not satisfy the PMS conditions (the parameters are shown above each sub-figure). Two PMS regions (a) and (b) are identified within the shock–sheath region whereas the third PMS region (d) is identified in the trailing solar wind. PMS structure evolution is rare in low plasma beta conditions, and this is reflected in our observations as well, i.e. we do not find any PMS characteristic associated with the MC crossing (region 3) (see sub-plot c in Fig. 2). Region 5 also does not exhibit any characteristics of PMS (see sub-plot e in Fig. 2). The observed PMSs, i.e. regions 1, 2, and 4, are inclined with angles of 79.13°, 85.02°, and 86.37° respectively with respect to the ecliptic plane. PMSs normal within the shock–sheath are mostly along the x-direction; however, the PMS after the MC has a normal in the x–y plane.

2.2 Alfvén-wave identification

The presence of Alfvén waves shows a good correlation between the change in the magnetic field and velocity components, i.e. the Walén relation (Walen 1944; Hudson 1971), which is as follows:

$$\delta V_{\rm A} = \frac{\delta B}{\sqrt{\mu_0 \rho}} \tag{1}$$

$$\delta V = |R_{\rm W}| \delta V_{\rm A} \tag{2}$$

where δB and δV are the fluctuations in the IMF and solar wind velocity vector components after subtracting the background. The Walén slope ($R_{\rm W}$) gives the liner relationship between δV and $\delta V_{\rm A}$ (Burlaga 1971; Yang et al. 2016). The accuracy of the Walén test is heavily influenced by the determination of the background magnetic field (B_0), but it is not an observable quantity. In the literature, the average value of the de Hoffmann–Teller (HT) frame or the mean value of the respective components is utilized (Gosling, Teh & Eriksson 2010; Yang & Chao 2013; Raghav & Shaikh 2018; Raghav et al. 2018; Raghav & Kule 2018). However, sometimes the average HT frame may not be appropriate, especially when many dynamic magnetic structures are present in the solar wind (Gosling et al. 2009; Li et al. 2016). Therefore, in this study, bandpass filters with different frequency bands are utilized in the plasma velocity and magnetic field observations to determine the pure fluctuations. We expect this to minimize the uncertainty in the Alfvén-wave identification. A similar technique has been used in the past (Li et al. 2016). We use the following frequency-band filters: 10s–15s, 15s–25s, 25s–40s, 40s–60s, 60s–100s, 100s–160s, 160s–250s, 250s–400s, 400s–630s, and 630s–1000s. For each bandpass signal the Walén relation is:

$$\delta V_i = \pm \delta V_{{\rm A}i} \tag{3}$$

where V_i and $V_{{\rm A}i}$ are the bandpass V (solar wind velocity) and $V_{\rm A}$ (local Alfvén velocity) components with the ith filter. The $\pm$ shows the propagation parallel and antiparallel to the background magnetic field. The correlation coefficient between V_i and $V_{{\rm A}i}$ confirms the existence of Alfvén waves or Alfvénic fluctuations in the region of examination. We have used 30 min time windows for the entire region of study. The correlation coefficient ($CC \geq 0.65$) for each frequency band is shown as a colour contour map in Fig. 3. The dark red colour map in all three components indicates the existence of Alfvén waves, whereas other colour contour regions suggest the presence of Alfvénic fluctuations. The empty contour map is interpreted as the absence of Alfvénic fluctuations.

Based on the above observations, Fig. 3 clearly shows that Alfvénic fluctuations are observed at the leading edge of the sheath (region 1), whereas their existence is reduced in the trailing part of region 1. Alfvénic fluctuations are absent in more than half of regions 2 and 3. Moreover, some parts of regions 2 and 3 demonstrate weak evidence of Alfvénic fluctuations in the selected frequency range. In fact, they are absent in the front part of region 4, but, their signature improves significantly in the trailing part of region 4, and substantial evidence is found in region 5.

3 RESULT AND DISCUSSION

We studied an ICME-induced geomagnetic storm that demonstrates complex features such as (i) decreasing and complete recovery phase during shock–sheath transit, (ii) gradual decrease but no recovery during MC crossing, and (iii) two different recovery phases (fast and slow phases) during trailing solar wind transit. It is also important to note that PMS is identified within the sheath region as well as in the trailing solar wind region. Moreover, Alfvénic fluctuations are identified in most of the ICME regions, and strong evidence of Alfvén waves is found in the trailing solar wind region. Therefore, we divided the complete storm temporal profile into five subsequent regions. Their important characteristics are summarized as follows (also see Fig. 4):

(i) Region 1 demonstrates the decreasing phase of the storm during sheath crossover with transit time (Δt) = 6.73 h in which SYM-H decreases from 30 to −69 nT.

(ii) Region 2 shows a recovery profile during sheath transit with Δt = 8.28 h in which SYM-H recovers from −69 to 0 nT.

(iii) Region 3 shows a slow and gradual decreasing phase during MC transit with Δt = 25.00 h in which SYM-H decreases from 0 to −101 nT.

(iv) Region 4 shows a recovery phase during trailing solar wind transit with Δt = 12.20 h in which SYM-H recovers from −101 to −27 nT.

Downloaded from https://academic.oup.com/mnras/article/490/3/3440/5610655 by Inter-University Centre for Astronomy and Astrophysics user on 04 May 2023

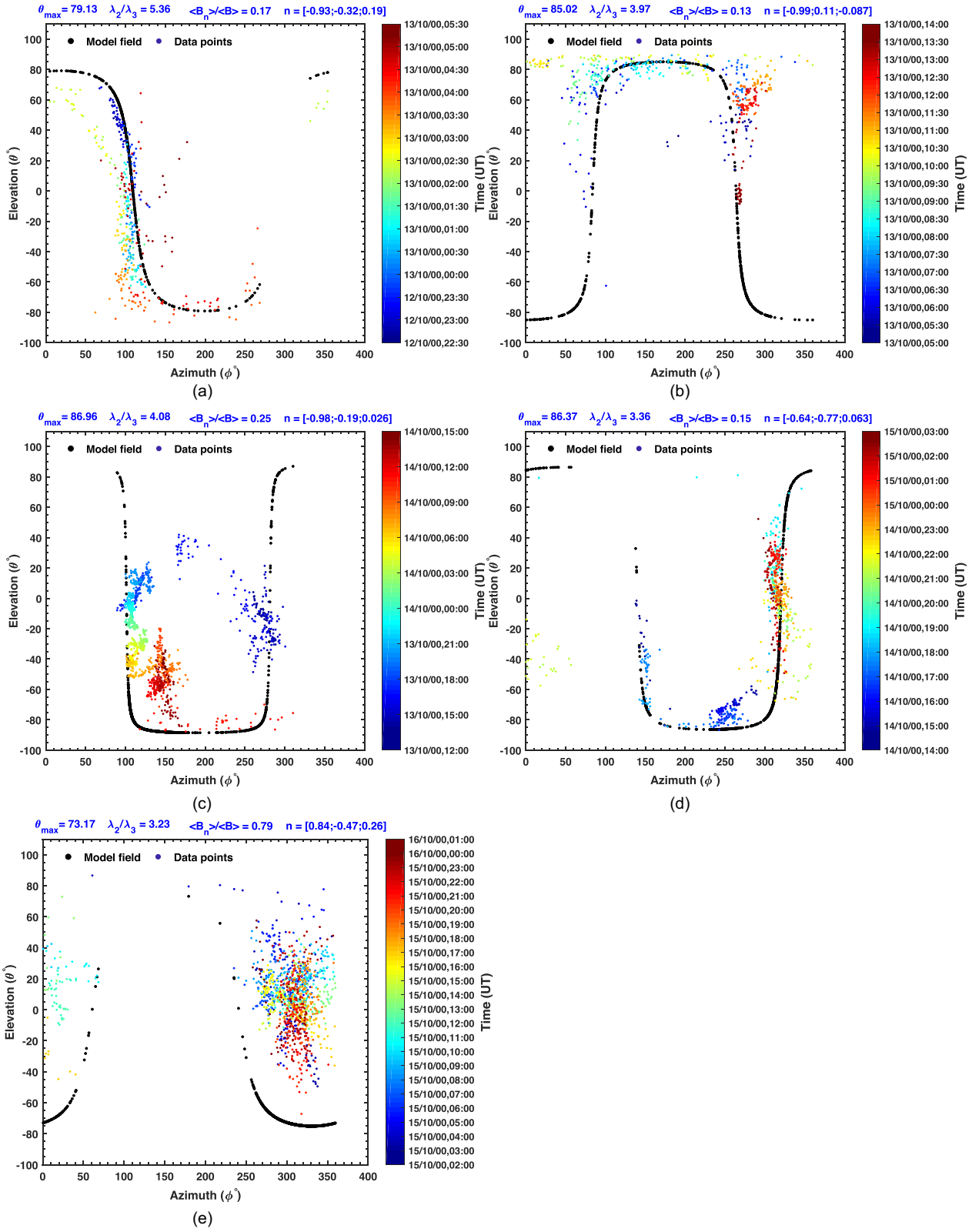

Figure 2. Distribution of azimuth (ϕ) versus elevation (θ) angle of IMF in GSE coordinates for different phases of the geomagnetic storm (as shown in Fig. 4): (a) Decreasing phase, (b) Fast recovery within the shock–sheath, (c) Gradual decreasing phase in magnetic cloud (MC), (d) Fast and (e) Slow recovery phase after MC crossing. $\frac{\lambda_2}{\lambda_3}$, $\frac{<B_n>}{B}$, and n give information about the planarity, efficiency, and normal direction of the PMS. $\theta_{\max}$ is the inclination of the PMS plane w.r.t. the ecliptic plane. When the IMF vectors $\vec{B} = (B_x, B_y, B_z) \equiv (B\cos\theta\cos\phi, B\cos\theta\sin\phi, B\sin\theta)$ are parallel to a plane whose normal is $\vec{n} \equiv (n_x, n_y, n_z)$, the relation between ϕ and θ is given as $n_x\cos\theta\cos\phi + n_y\cos\theta\sin\phi + n_z\sin\theta = 0$ (Nakagawa et al. 1989; Palmerio et al. 2016). The above curve fitting (see the black dotted curve) to the measured (dotted coloured plot) ϕ and θ indicates the presence of PMS.

Downloaded from https://academic.oup.com/mnras/article/490/3/3440/5610655 by Inter-University Centre for Astronomy and Astrophysics user on 04 May 2023

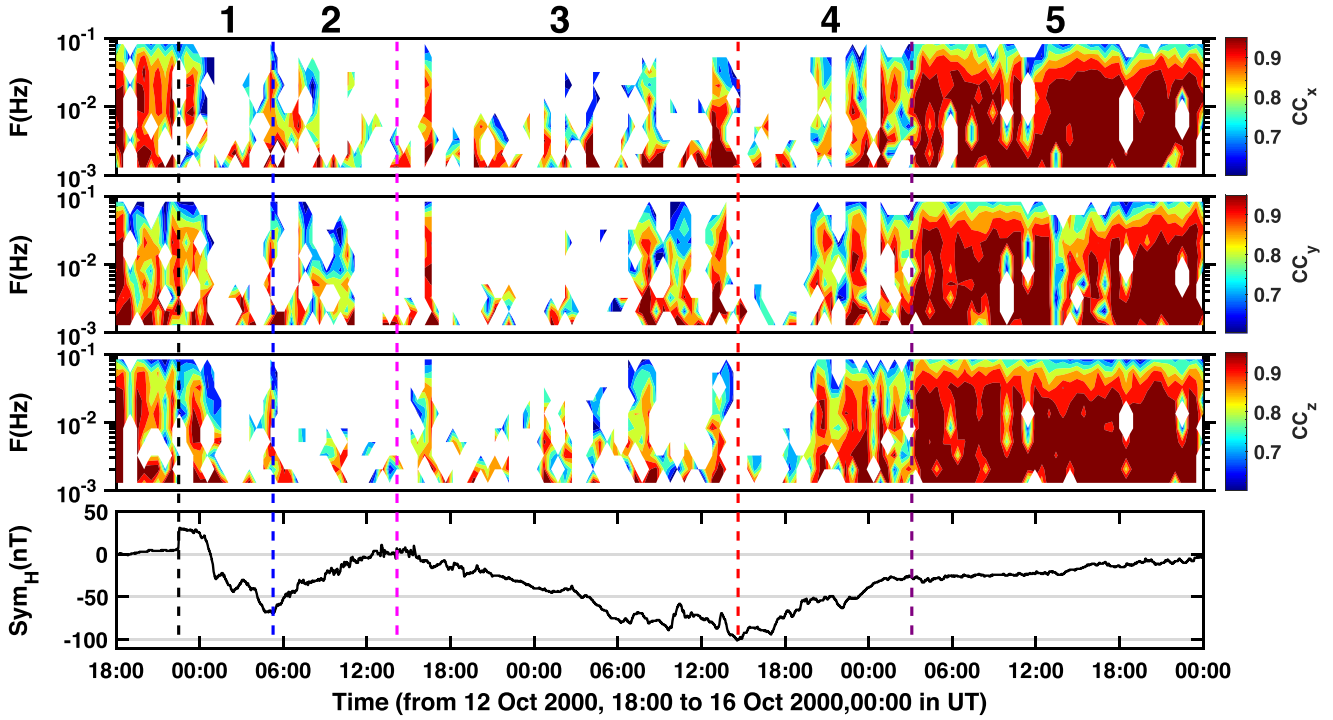

Figure 3. This figure demonstrates the time–frequency distribution of the correlation coefficient between V_{Ai} and V_i for the complete event. The numbers from one to five indicate different phases of the geomagnetic storm that occurred on 2000 October 12 (see the bottom SYM-H plot). 3 s time resolution data from the *Wind* spacecraft are utilized.

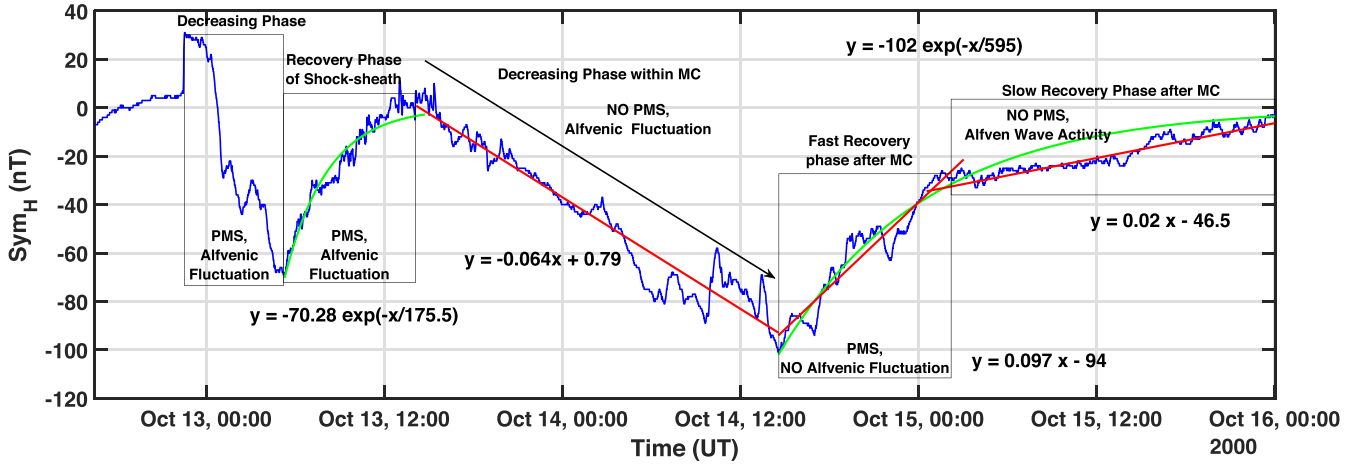

Figure 4. Geomagnetic storm occurring on 2000 October 12. The different phases of the storm are indicated in the box.

(v) Region 5 shows a slow recovery phase during trailing solar wind transit with $\Delta t = 21.65$ h in which SYM-H recovers from -27 to 0 nT.

Generally, the duration of the main phase is typically 2–8 h while that of the recovery phase is as short as 8 h or as long as 7 d (Gonzalez et al. 1994; Kamide et al. 1998; Kilpua et al. 2017b). Therefore, region 1 manifested as a fast decrease phase whereas region 2 and 4 are ascribed as fast recovery phases of the storm. To understand the recovery phase in detail, researchers have used either hyperbolic and/or exponential fitting functions. The exponential model is based on the following hypothesis: (i) energy injection is negligible once the recovery phase starts, (ii) τ is constant, and (iii) the D_{st} index represents the magnetic perturbations induced by the activity of the ring-current system (Burton, McPherron & Russell 1975; O'Brien & McPherron 2000; Dasso, Gómez & Mandrini 2002; Wang, Chao & Lin 2003). Therefore, the recovery phase is represented as:

$$D_{st} = D_{st,0} \exp[t/\tau] \quad (4)$$

where $1/\tau$ gives the degree of reduction of the exponential function. τ indicates the characteristic recovery time (dependent on $D_{st,0}$ and the time lapse). Based on this fitting model, Burton et al. (1975) and Dasso et al. (2002) reported $\tau = 7$ h and 14 ± 4 h. Pudovkin, Zaitseva & Sizova (1985) studied a moderate storm, i.e. -120 nT $< D_{st,min} < -50$ nT, and reported a value of τ in between 7 and

Downloaded from https://academic.oup.com/mnras/article/490/3/3440/5610655 by Inter-University Centre for Astronomy and Astrophysics user on 04 May 2023

17 h. Moreover, Feldstein (1992) summarized various studies on the decay time of the recovery phase and indicated a large dispersion in the reported decay time (Gonzalez et al. 1989; Mac-Mahon & Gonzalez 1997; Vassiliadis et al. 1999; O'Brien & McPherron 2000).

In our work, we have used the SYM-H index instead of the D_{st} index. The recovery phase associated with region 2 (see the green fitted curve in Fig. 4) follows an exponential fit, i.e. $y = -70.28e^{-x/175.5}$; here $\tau = 175.5$ min $= 2.93$ h. Similarly, we have fitted the complete recovery profile after MC transit (regions 4 and 5; see the green fitted curve in Fig. 4). We found an exponential fit, i.e. $y = -102e^{-x/595}$; here $\tau = 595$ min $= 9.92$ h. It is clear that the initial recovery rate was fast (region 4), but suddenly it slowed down in region 5. Therefore, we also performed a linear fitting independently for regions 4 and 5. We found that region 4 is best fitted with $y = 0.097x - 94$, and region 5 with $y = 0.02x - 46.5$. The slope of the fit indicates that the recovery trend associated with region 4 is steeper than that of region 5, i.e. region 4 recovers faster than region 5. In addition to this, region 3 shows a gradual decrease of SYM-H profile, which is completely inconsistent with reported storms in the literature. Therefore, we have also fitted region 3 (complete MC transit). The decreasing trend of region 3 follows a linear trend (Fig. 4, red fitted line), i.e. $y = -0.064x + 0.79$. The slow and gradual decreasing trend in IMF B_z could be the primary driver of the observed SYM-H profile.

Our analysis concludes that regions 1, 2 and 4 are exhibiting features of PMSs. It is also possible that regions 1 and 2 could be part of a single PMS. The amplification and alignment of solar wind discontinuities near the ICME-driven shock or the draping of the magnetic field lines around the ICME MC is the cause of PMS generation (Palmerio et al. 2016; Shaikh et al. 2018). The shock–sheath may be transformed to PMS by compression with lateral expansion of the ICME (Neugebauer et al. 1993). Moreover, the measured plasma parameters and magnetic field after MC transit suggest that the studied event is followed by another CME-like structure (see the plasma beta value and solar wind variation). Therefore, the identified PMSs after the end of the magnetic cloud could be caused by CME–CME interaction. However, detailed study is needed in this direction. It will throw some light on the origin of PMSs. The draping of plasma accompanied by compression leads to an enhancement of the out-of-ecliptic field component (B_z) at the cost of the ecliptic components (B_x, B_y) (McComas et al. 1988, 1989). Kataoka et al. (2015) and Palmerio et al. (2016) suggest that the draping of the plasma causes intense and prolonged negative B_z, to explain the PMS-induced enhanced geo-effectiveness of the storm. In the present study, we opine that the observed fast decrease or recovery in regions 1, 2 and 4 is caused by the high compression and sudden transition of the IMF B_z from the southward to the northward direction (for recovery) or vice versa (for the decrease) within the PMS. An enhanced decrease in the D_{st}/SYM-H index during PMS is reported in the literature (Kataoka et al. 2015), whereas the present study explicitly demonstrates the PMS contribution to the fast recovery phase of the storm.

Our analysis indicates the presence of Alfvénic fluctuations during the MC (region 3) and region 5 transit. Tsurutani & Gonzalez (1987) found that high-intensity ($AE > 1000$ nT) long-duration ($T >$ 2 d) continuous aurora1 activity (HILDCAA) events are associated with interplanetary Alfvén waves. Zhang et al. (2014) reported that Alfvén waves superposed southward B_z triggered geomagnetic storms and sub-storms. Raghav et al. (2018, 2019) reported that the presence of torsional Alfvén waves in a magnetic cloud contributes to the long recovery time of geomagnetic storms. Here, they hypothesized that the Alfvén waves might extend the southward IMF B_z and supply consistent energy/plasma to the magnetosphere by the magnetic reconnection process. Therefore, we opine that Alfvén waves may be the cause of the slow decrease/recovery during the studied storm. A detailed investigation to understand the effect of Alfvén waves on the extended main and recovery phases of the geomagnetic storm is needed.

ACKNOWLEDGEMENTS

We are grateful to the *Wind* spacecraft data providers (wind.nasa.gov) for making the interplanetary data available. The authors also thank the OMNI database for providing the geomagnetic index data. The authors extend their thanks to the Indian Institute of Geomagnetism (IIG) for constant support for the work. AB is currently supported by the NASA Living with a Star Jack Eddy Postdoctoral Fellowship Program, administered by UCAR's Cooperative Programs for the Advancement of Earth System Science (CPAESS).

REFERENCES

Akasofu S.-I., 1963, Space Sci. Rev., 2, 91
Akasofu S.-I., 2011, Space Sci. Rev., 164, 85
Akasofu S.-I., 2018, Int. J. Earth Sci. Geophysics, 4:018
Akasofu S.-I., Chapman S., Venkatesan D., 1963, J. Geophysical Res., 68, 3345
Akasofu S.-I., Chapman S., Meng C.-I., 1965, J. Atmos. Terr. Phys., 27, 1275
Axford W. I., Hines C. O., 1961, Canadian J. Phys., 39, 1433
Belcher J., Davis L. Jr, 1971, J. Geophysical Res., 76, 3534
Bhaskar A., Vichare G., Arunbabu K., Raghav A., 2016a, Ap&SS, 361, 242
Bhaskar A., Subramanian P., Vichare G., 2016b, ApJ, 828, 104
Bruno R., Carbone V., 2013, Living Rev. Sol. Phys., 10, 2
Burlaga L., Sittler E., Mariani F., Schwenn R., 1981, J. Geophysical Res. Space Phys., 86, 6673
Burlaga L., Lepping R., Jones J., 1990, Physics of Magnetic Flux Ropes, AGU Geophysical monograph no 58. Wiley, New York, p. 373
Burlaga L. F., 1971, J. Geophysical Res., 76, 4360
Burton R. K., McPherron R., Russell C., 1975, J. Geophysical Res., 80, 4204
Chapman S., 1933, Terr. Magn. Atmos. Electricity, 38, 79
Chapman S., Bartels J., 1940, Geomagnetism: Geomagnetic and Related Phenomena, Vol. 1. Clarendon, Oxford
Chapman S., Ferraro V. C., 1931, Terr. Magn. Atmos. Electricity, 36, 77
Cramer N. F., 2011, The Physics of Alfven Waves. Wiley, New York
Daglis I. A., Thorne R. M., Baumjohann W., Orsini S., 1999, Rev. Geophysics, 37, 407
Dasso S., Gómez D., Mandrini C. H., 2002, J. Geophysical Res. Space Phys., 107, SMP–5
Davis T. N., Sugiura M., 1966, J. Geophysical Res., 71, 785
Dessler A., Francis W., Parker E., 1960, J. Geophysical Res., 65, 2715
Dungey J. W., 1961, Phys. Rev. Lett., 6, 47
Eastwood J., Lucek E., Mazelle C., Meziane K., Narita Y., Pickett J., Treumann R., 2005, Outer Magnetospheric Boundaries: Cluster Results. Springer, Berlin, p. 41
Fairfield D. H., Cahill L. J. Jr, 1966, J. Geophysical Res., 71, 155
Feldstein Y. I., 1992, Space Sci. Rev., 59, 83
Feng H., Wu D., Lin C., Chao J., Lee L., Lyu L., 2008, J. Geophysical Res. Space Phys., 113, A12105
Frank L. A., 1967, J. Geophysical Res., 72, 3753
Gonzalez W., Joselyn J. A., Kamide Y., Kroehl H. W., Rostoker G., Tsurutani B., Vasyliunas V., 1994, J. Geophysical Res. Space Phys., 99, 5771
Gonzalez W. D., Tsurutani B. T., 1987, Planet. Space Sci., 35, 1101
Gonzalez W. D., Tsurutani B. T., Gonzalez A. L., Smith E. J., Tang F., Akasofu S.-I., 1989, J. Geophysical Res. Space Phys., 94, 8835

Downloaded from https://academic.oup.com/mnras/article/490/3/3440/5610655 by Inter-University Centre for Astronomy and Astrophysics user on 04 May 2023

Gonzalez W. D., Tsurutani B. T., De Gonzalez A. L. C., 1999, Space Sci. Rev., 88, 529
Gosling J., Bame S., McComas D., Phillips J., 1990, Geophysical Res. Lett., 17, 901
Gosling J., McComas D., Roberts D., Skoug R., 2009, ApJ, 695, L213
Gosling J., Teh W.-L., Eriksson S., 2010, ApJ, 719, L36
Guarnieri F., 2006, Recurrent Magnetic Storms: Corotating Solar Wind Streams. Wiley, New York, p. 235
Hakamada K., 1998, Sol. Phys., 181, 73
Hansen R. T., Hansen S. F., Sawyer C., 1976, Planet. Space Sci., 24, 381
Hudson P., 1971, Planet. Space Sci., 19, 1693
Huttunen K., Koskinen H., 2004, Ann. Geophysicae, 22, 1729
Huttunen K., Koskinen H., Karinen A., Mursula K., 2006, Geophysical Res. Lett., 33, L06107
Huttunen K. E. J., Koskinen H. E., Schwenn R., 2002, J. Geophysical Res. Space Phys., 107, SMP 20–1-8
Jones G., Balogh A., Horbury T., 1999, Geophysical Res. Lett., 26, 13
Jones G., Rees A., Balogh A., Forsyth R., 2002, Geophysical Res. Lett., 29, 15
Jones G. H., Balogh A., 2001, The 3-D Heliosphere at Solar Maximum. Springer, Berlin, p. 165
Kamide Y. et al., 1998, J. Geophysical Res. Space Phys., 103, 17705
Kasahara Y., Miyoshi Y., Omura Y., Verkhoglyadova O., Nagano I., Kimura I., Tsurutani B., 2009, Geophysical Res. Lett., 36, L01106
Kataoka R., Shiota D., Kilpua E., Keika K., 2015, Geophysical Res. Lett., 42, 5155
Keika K., Nosé M., Brandt P., Ohtani S., Mitchell D., Roelof E., 2006, J. Geophysical Res. Space Phys., 111, A11S12
Kilpua E., Koskinen H. E., Pulkkinen T. I., 2017a, Living Rev. Sol. Phys., 14, 5
Kilpua E., Balogh A., von Steiger R., Liu Y., 2017b, Space Sci. Rev., 212, 1271
Kozyra J., Jordanova V., Home R., Thorne R., 1997, Magnetic Storms, AGU: Geophysical Monograph Series 98. Wiley, New York, p. 187
Kozyra J. U., Liemohn M. W., 2003, Magnetospheric Imaging: The Image Prime Mission. Springer, Berlin, p. 105
Krieger A., Timothy A., Roelof E., 1973, Sol. Phys., 29, 505
Lepping R., Behannon K., 1980, J. Geophysical Res. Space Phys., 85, 4695
Lepping R. et al., 1997, J. Geophysical Res. Space Phys., 102, 14049
Li H., Wang C., Chao J., Hsieh W., 2016, J. Geophysical Res. Space Phys., 121, 42
Lindsay G., Russell C., Luhmann J., 1995, J. Geophysical Res. Space Phys., 100, 16999
Lugaz N., Farrugia C., Winslow R., Al-Haddad N., Kilpua E., Riley P., 2016, J. Geophysical Res. Space Phys., 121, 10861
Mac-Mahon R. M., Gonzalez W., 1997, J. Geophysical Res. Space Phys., 102, 14199
Manchester W. IV et al., 2005, ApJ, 622, 1225
Marsch E., 2006, Living Rev. Sol. Phys., 3, 1
McComas D., Gosling J., Winterhalter D., Smith E., 1988, J. Geophysical Res. Space Phys., 93, 2519
McComas D., Gosling J., Bame S., Smith E., Cane H., 1989, J. Geophysical Res. Space Phys., 94, 1465
Milan S., Gosling J., Hubert B., 2012, J. Geophysical Res. Space Phys., 117, A03226
Moldwin M., Ford S., Lepping R., Slavin J., Szabo A., 2000, Geophysical Res. Lett., 27, 57
Nakagawa T., 1993, Sol. Phys., 147, 169
Nakagawa T., Nishida A., Saito T., 1989, J. Geophysical Res. Space Phys., 94, 11761
Neugebauer M., Clay D., Gosling J., 1993, J. Geophysical Res. Space Phys., 98, 9383
O'Brien T. P., McPherron R. L., 2000, J. Geophysical Res. Space Phys., 105, 7707
Oliveira D. M., Raeder J., 2014, J. Geophysical Res. Space Phys., 119, 8188
Palmerio E., Kilpua E. K., Savani N. P., 2016, Ann. Geophysicae, 34, 313
Prölss G., 1973, Planet. Space Sci., 21, 983
Pudovkin M., Zaitseva S., Sizova L., 1985, Planet. Space Sci., 33, 1097
Pulkkinen T. I., Partamies N., Huttunen K., Reeves G., Koskinen H., 2007, Geophysical Res. Lett., 34, L02105
Raghav A., Bhaskar A., Lotekar A., Vichare G., Yadav V., 2014, J. Cosmology Astroparticle Phys., 2014, 074
Raghav A., Shaikh Z., Bhaskar A., Datar G., Vichare G., 2017, Sol. Phys., 292, 99
Raghav A. N., Kule A., 2018, MNRAS, 480, L6
Raghav A. N., Shaikh Z. I., 2018, preprint (arXiv:1810.06004)
Raghav A. N., Kule A., Bhaskar A., Mishra W., Vichare G., Surve S., 2018, ApJ, 860, 26
Raghav A. N., Choraghe K., Shaikh Z. I., 2019, MNRAS, 488, 910
Reames D. V., 1999, Space Sci. Rev., 90, 413
Richardson I. et al., 2006, J. Geophysical Res. Space Phys., 111, A07S09
Richardson I. G., 2018, Living Rev. Sol. Phys., 15, 1
Sanderson T., Erdös G., Balogh A., Forsyth R., Marsden R., Gosling J., Phillips J., Tranquille C., 2000, J. Geophysical Res. Space Phys., 105, 18275
Shaikh Z., Raghav A., Bhaskar A., 2017, ApJ, 844, 121
Shaikh Z. I., Raghav A. N., Vichare G., Bhaskar A., Mishra W., 2018, ApJ, 866, 118
Sheeley N., Harvey J., Feldman W., 1976, Sol. Phys., 49, 271
Siscoe G., Odstrcil D., 2008, J. Geophysical Res. Space Phys., 113, A00B07
Smith P., Hoffman R. A., 1973, J. Geophysical Res., 78, 4731
Sonnerup B. U., Scheible M., 1998, Analysis Methods for Multi-Spacecraft Data. ISSI Scientific Report, Switzerland, p. 185
Tsurutani B., Lakhina G., Verkhoglyadova O. P., Gonzalez W., Echer E., Guarnieri F., 2011, J. Atmos. Sol. Terr. Phys., 73, 5
Tsurutani B. T., Gonzalez W. D., 1987, Planet. Space Sci., 35, 405
Tsurutani B. T., Gonzalez W. D., 1997, Magnetic Storms, AGU, Geophysical monograph series 98. Wiley, New York, p. 77
Tsurutani B. T., Gonzalez W. D., Tang F., Akasofu S. I., Smith E. J., 1988, J. Geophysical Res. Space Phys., 93, 8519
Tsurutani B. T. et al., 2006, J. Geophysical Res. Space Phys., 111, A07S01
Vassiliadis D., Klimas A., Valdivia J., Baker D., 1999, J. Geophysical Res. Space Phys., 104, 24957
Walen C., 1944, Arkiv Astron., 30, 1
Wang C., Chao J., Lin C.-H., 2003, J. Geophysical Res. Space Phys., 108, 1341
Webb D. F., Howard T. A., 2012, Living Rev. Sol. Phys., 9, 3
Williams D., 1983, in Progress in Solar-Terrestrial Physics. Springer, Berlin, p. 223
Yang L., Chao J., 2013, Chinese J. Space Sci., 33, 353
Yang L., Lee L., Chao J., Hsieh W., Luo Q., Li J., Shi J., Wu D., 2016, ApJ, 817, 178
Yermolaev Y. I., Lodkina I., Nikolaeva N., Yermolaev M. Y., 2012, J. Geophysical Res. Space Phys., 117, A08207
Zhang X.-Y., Moldwin M., Steinberg J., Skoug R., 2014, J. Geophysical Res. Space Phys., 119, 3259
Zurbuchen T. H., Richardson I. G., 2006, Coronal Mass Ejections. Springer, Berlin, p. 31

This paper has been typeset from a TEX/LATEX file prepared by the author.

Downloaded from https://academic.oup.com/mnras/article/490/3/3440/5610655 by Inter-University Centre for Astronomy and Astrophysics user on 04 May 2023